Journal of Coastal Research	33	3	518–530	Coconut Creek, Florida	May 2017

Assessment of Storm Surge along the Coast of Central Vietnam

Nguyen Ba Thuy[†]*, Sooyoul Kim[‡], Do Dinh Chien[§], Vu Hai Dang[††], Hoang Duc Cuong[†], Cecilie Wettre[‡‡], and Lars Robert Hole[‡‡]

[†]Vietnam National Hydrometeorolocical Forecasting Center
Hanoi, Vietnam

[‡]Graduate School of Engineering
Tottori University
Tottori 680-850, Japan

[§]Vietnam Institute of Meteorology, Hydrology and Climate Change
Hanoi, Vietnam

[††]Institute of Marine Geophysics and Geology
Hanoi, Vietnam

[‡‡]Division of Oceanography and Maritime Meteorology
Norwegian Meteorological Institute
Bergen, Norway

www.cerf-jcr.org

www.JCRonline.org

ABSTRACT

Thuy, N.B.; Kim, S.; Chien, D.D.; Dang, V.H.; Cuong, H.D.; Wettre, C., and Hole, L.R., 2017. Assessment of storm surge along the coast of central Vietnam. *Journal of Coastal Research,* 33(3), 518–530. Coconut Creek (Florida), ISSN 0749-0208.

In the present paper, the interaction of surge, wave, and tide along the coast of central Vietnam is assessed using a coupled model of surge, wave, and tide. A series of storm surge simulations for Typhoons Xangsane (2006), Ketsana (2009), and Nary (2013) are carried out, considering the effects of tides and waves that combines wave-dependent drag and wave-induced radiation stress to find a predominant factor in storm surge generation. The results indicate that the surge–wave interaction is crucial to the storm surge simulation in this area. In particular, the wave-dependent drag improves an accuracy of the storm surge level up to 30%. In addition, the radiation stress contributes up to 15%. However, the tide–surge interaction is negligible because there is less than 2% difference in results with and without the tide. A series of coupled surge and wave simulations for 49 historical typhoons in the period of 1951 to 2014 show that mean peak surge levels along the coast are 2.5 m. The highest peak surge level reached 4.1 m at Cuaviet in the Quangtri Province during Typhoon Harriet (1971).

ADDITIONAL INDEX WORDS: *Typhoon; coupled model of surge, wave, and tide; interaction of surge.*

INTRODUCTION

The Intergovernmental Panel on Climate Change's 5th Assessment Report (Field *et al.*, 2014) found that global climate change accelerates the activity of tropical cyclones (TCs), making them more intensive with accompanying severe storm surges. In recent years, the weather and hydrological phenomena in Vietnam have become more variable: the maximum daily rainfall trend is increasing and the frequency of TCs is rising on the south coast of Vietnam (*e.g.*, Tan and Thanh, 2013). Thus, the coastal areas are increasingly exposed to coastal disasters, such as strong wind, heavy rain, high waves, and storm surges. Storm surges due to typhoons, such as Typhoons Linda (1997), Wukong (2000), Chanchu (2006), Xangsane (2006), and Ketsana (2009), are catastrophic events, causing severe damage to ocean and coastal communities (Thanh, 2011). Typhoon Dan (1989) generated a record-breaking peak surge level of 3.6 m in the Province of Hatinh (Thanh, 2011). To mitigate potential storm surge damage, understanding storm surge is crucial for the planning of coastal facilities and activities.

To assess storm surges, there are two conventional types of physics-based numerical models: a decoupled model of storm surge and a coupled model of surge, wave, and tide (SuWAT). In the last three decades, coupled models have been given attention, especially those focusing on the interaction of surge, wave, and tide. Several studies have introduced wind stress as a function of waves (Janssen, 1989, 1991). Since then, a number of studies that examined wave-induced stress directly obtained in coupled models of surge and wave showed the significant improvements of the model results compared with observation data (*e.g.*, Funakoshi, Hagen, and Bacopoulos, 2008; Kim, Yasuda, and Mase, 2008; Zhang and Li, 1997). Wave setup driven by a force of the divergence of radiation stress in the nearshore has also been studied with coupled models of surge and wave (*e.g.*, Bertin *et al.*, 2015; Kim, Yasuda, and Mase, 2010; Mastenbroek, Burgers, and Janssen, 1993). It was found that the wave setup induced by the force of the radiation stress was substantial in the peak surge level during Typhoon Anita (1970; *e.g.*, Kim, Yasuda, and Mase, 2010). It was found that the tide–surge interaction is not negligible when estimating local surge levels (*e.g.*, Chen, Wang, and Zhao, 2008; Choi, Eum, and Woo, 2003; Kim, Yasuda, and Mase, 2008). Besides the interaction of surge, wave, and tide, topographic characteristics (*e.g.*, bed slope) play an important role in the increase or decrease of wave setup, runup, and wind-driven surge (*e.g.*, Dietrich *et al.*, 2010; Kennedy *et al.*, 2012).

For several decades, climate change impact studies have focused on storm surge studies in Vietnam (*e.g.*, Ninh, 1992; Sao, 2008; Thang, 1999; Thuy, 2003). Conventional two-dimensional (or three-dimensional), nonlinear shallow-water equations have been used. In other words, other factors, such as tides and waves, were not taken into account in the storm surge model in those studies. Recently, the effect of waves on storm surge has been investigated in Vietnam. Hien *et al.* (2010) showed using an empirical formula that the wave setup

DOI: 10.2112/JCOASTRES-D-15-00248.1 received 28 December 2015; accepted in revision 21 June 2016; corrected proofs received 26 August 2016; published pre-print online 21 October 2016.
*Corresponding author: thuybanguyen@gmail.com

induced by the force of the divergence of radiation stress is significant in the storm surge on the coast of Haiphong. Thuy *et al*. (2014) found that the Typhoon Kalmaegi (2014) surge was significantly influenced by waves on the Haiphong coast, obtained from numerical simulations using SuWAT.

In the present study, primary factors affecting storm surge on the middle coast of Vietnam are quantitatively investigated using SuWAT. The study highlights that coupling processes between surge and wave are critical to the prediction of storm surge on the coast of central Vietnam and that only using SuWAT (developed by Kim, Yasuda, and Mase, 2008) can accurately estimate storm surges. A series of storm surge simulations are conducted for Typhoons Xangsane (2006), Ketsana (2009), and Nary (2013) that considers the interaction of surge, wave, and tide. Then, historical storm surges of 49 typhoons in the period of 1951 to 2014 are assessed. All typhoon data in this study are collected from the Regional Specialized Meteorological Center (RSMC) Best Track Data of the Japan Meteorological Agency (JMA, 2016).

In this study, the coastal area from the Provinces of Quangbinh to Quangnam (Figure 1a) was selected. This is where the most severe storm surges have occurred on the Vietnam coast. Although the frequency of typhoons in this area is 0.8 per year on average, great inundations occurred due to Typhoons Becky (1990), Xangsane (2006), and Ketsana (2009) (Thanh, 2011) because of a bathymetry feature in the area where there is shallow water in open sea and a low-lying area with no coastal structures.

The frequency of typhoons in terms of the Beaufort scale of wind (WMO Staff, 1998) in the study area is summarized in Table 1. In the period of 1951 to 2014, the frequency of typhoon intensity larger than level 12 is 28.3% in total and the typhoon frequency for intensity of larger than level 10 is dominantly 47.2%. Relative large surge levels were computed from the tidal gauge data in this area, for instance, 1.7 m at Thanhkhe in the Province of Quangbinh (Typhoon Cecil, 1975), 1.8 m at Cuagianh (Typhoon Becky, 1990), 1.5 m at Sontra (Typhoon Xangsane, 2006), and 2.4 m at Hoian (Typhoon Ketsana, 2009) (Thanh, 2011). Otherwise, higher surge levels were not measured because of lack of either measurement devices or field surveys. For example, Typhoon Harriet (1971) is the most intense typhoon in the history of Vietnam, but there are no observations. To examine a critical factor in the generation of storm surge in the study area, the representative Typhoons Xangsane (2006), Ketsana (2009), and Nary (2013) were selected. The typhoon tracks are provided in Figure 1b.

Because of the open sea in the region of interest, waves accompanying the typhoon devastate coastal infrastructures in low-lying areas. The maximum wave height reached 6.0 m at Sontra in the Province of Danang (Figure 1b) during Typhoon Xangsane. Such waves may potentially cause a wave setup in shallow-water regions during typhoon events. Therefore, in the surge and wave simulation, the wave-induced radiation stress is considered.

In the study area, tidal cycles are semidiurnal and tidal amplitudes tend to decrease from the northern coast of the Province of Quangbinh to the middle coast of Hue, and then increase to the southern coast of the Province of Quangnam as shown in Figure 1a. In this region, the largest amplitudes in the Provinces of Quangbinh and Quangnam are approximately 0.9 m. In other words, the maximum tidal range is up to 1.8 m. Therefore, the tide is also taken into account in the simulation.

METHODS

To analyze the storm surge in the study area, the coupled SuWAT model developed by Kim, Yasuda, and Mase (2008) was used. SuWAT is capable of doing parallel computations for an arbitrary number of domains using the message passing interface. In the present study, three modules of surge, wave, and tide are integrated in SuWAT as shown in Figure 2, which reveals the information flow among modules and domains. The tidal module provides only boundary conditions to the surge modules in the outermost domain. Coupling parameters include open boundary values, internal exchange among modules, and domains in a machine. Calculations are sequentially carried out from the higher-level domain to the lower level; the rest of the lower-level domains waits for the completion of the higher-level domain at a time step. This modeling system has been implemented and verified in other studies (*e.g*., Kim, Yasuda, and Mase, 2010; Kim *et al*., 2014, 2015; Mase *et al*., 2011).

Surge Module

The surge module solves the depth-averaged, nonlinear shallow-water equations using the staggered Arakawa C grid in space and the leapfrog scheme in time. The explicit finite difference scheme is used with the upwind method:

$$\frac{\partial \eta}{\partial t}+\frac{\partial M}{\partial x}+\frac{\partial N}{\partial y}=0 \tag{1}$$

$$\begin{aligned}&\frac{\partial M}{\partial t}+\frac{\partial}{\partial x}\left(\frac{M^2}{d}\right)+\frac{\partial}{\partial y}\left(\frac{MN}{d}\right)+gd\frac{\partial \eta}{\partial x}\\&\quad=fN-\frac{1}{\rho_w}d\frac{\partial P}{\partial x}+\frac{1}{\rho_w}(\tau_S^x-\tau_b^x-F_x)+A_h\left(\frac{\partial^2 M}{\partial x^2}+\frac{\partial^2 M}{\partial y^2}\right)\end{aligned} \tag{2}$$

$$\begin{aligned}&\frac{\partial N}{\partial t}+\frac{\partial}{\partial y}\left(\frac{N^2}{d}\right)+\frac{\partial}{\partial x}\left(\frac{NM}{d}\right)+gd\frac{\partial \eta}{\partial y}\\&\quad=-fM-\frac{1}{\rho_w}d\frac{\partial P}{\partial y}+\frac{1}{\rho_w}(\tau_S^y-\tau_b^y-F_y)+A_h\left(\frac{\partial^2 N}{\partial x^2}+\frac{\partial^2 N}{\partial y^2}\right)\end{aligned} \tag{3}$$

where η is the sea surface level, M and N are the components of depth-integrated velocity in the horizontal and vertical directions, P is the atmospheric pressure, f is the Coriolis parameter, g is the gravitational acceleration, d is the total water depth $(\eta+h)$, A_h is the horizontal eddy diffusions, and ρ_w is the density of water. In addition, F_x and F_y represent the components of wave force, which correspond to the gradients of wave-induced radiation stress:

$$F_x=\frac{-\partial S_{xx}}{\partial x}-\frac{\partial S_{xy}}{\partial y} \tag{4}$$

$$F_y=\frac{-\partial S_{yx}}{\partial x}-\frac{\partial S_{yy}}{\partial y} \tag{5}$$

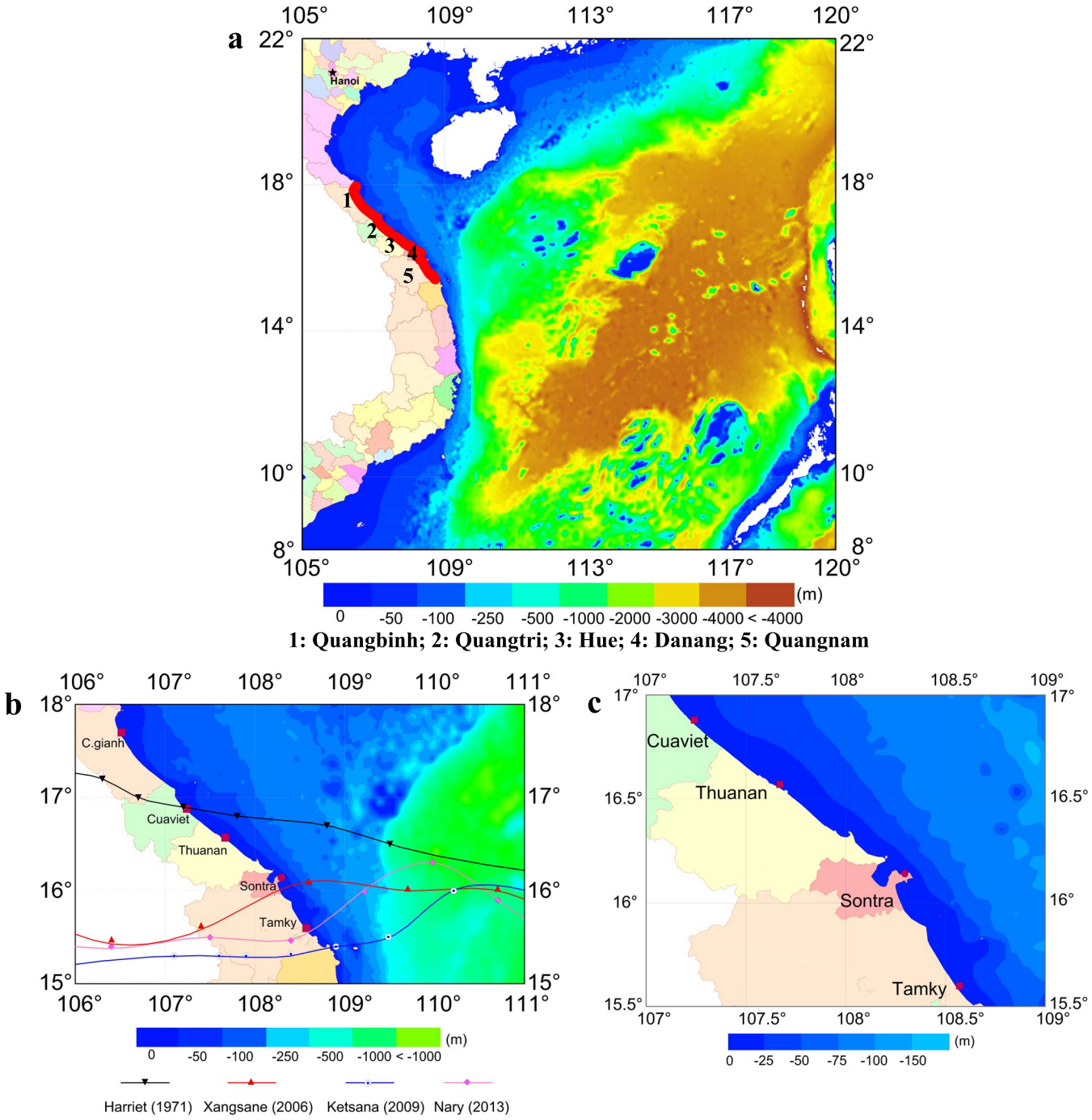

Figure 1. Geophysical domains of the study area with three levels. (a) Outermost domain of the Vietnam coast. (b) Intermediate domain with stations for tide (Cuagianh, Cuaviet, Thuanan, Sontra, and Tamky), meteorology (Thuanan and Sontra), and tracks (Typhoons Xangsane, Ketsana, Nary, and Harriet). (c) Innermost domain. (Color for this figure is available in the online version of this paper.)

Here, the wave radiation stresses are expressed by

$$S_{xx} = \rho g \iint \left[\frac{C_g}{C}\cos^2\theta + \frac{C_g}{C} - \frac{1}{2}\right] E d\sigma d\theta \tag{6}$$

$$S_{xy} = S_{yx} = \rho g \iint [\cos\theta \sin\theta] E d\sigma d\theta \tag{7}$$

$$S_{yy} = \rho g \iint \left[\frac{C_g}{C}\sin^2\theta + \frac{C_g}{C} - \frac{1}{2}\right] E d\sigma d\theta \tag{8}$$

where C and C_g are the wave velocity and the group velocity, respectively; σ and θ are the angular frequency and the wave direction, respectively; and E is the energy density spectrum.

Table 1. *Typhoon frequency according to a wind speed scale (Beaufort scale) in the study area (period: 1951–2014).*

Storm Level (Beaufort scale)	Wind Speed (m/s)	Typhoon Frequency (%) in Provinces					
		Quangbinh	Quangtri	Hue	Danang	Quangnam	Total
Under level 8	<17.8	9.4	5.7	3.8	0	7.5	26.4
Levels 8–9	17.9–22.0	15.1	1.8	1.9	5.7	1.9	26.4
Levels 10–11	22.1–30.9	9.4	1.9	1.9	1.9	3.8	18.9
Levels ≥12	>31.0	13.2	3.8	0	1.9	9.4	28.3

A conventional quadratic law is applied to the sea surface and bottom boundary layers. The bottom stress is computed by

$$\tau_b = \rho_w g n^2 \frac{\vec{Q}|\vec{Q}|}{d^{7/3}} \tag{9}$$

in which $\vec{Q}$ is the depth-integrated velocity vector and n is the Manning number (0.025) in all domains, as determined by Chien (2015). The wind stress is usually estimated by the following equation:

$$\tau_S = \rho_a C_D \vec{U}_{10}|\vec{U}_{10}| \tag{10}$$

where ρ_a is the density of air, C_D is the drag coefficient, and $\vec{U}_{10}$ is the wind speed at a 10-m height.

In a series of storm surge simulations, two C_Ds are used. One is conventional C_D (Honda and Mitsuyasu, 1980):

$$C_D = \begin{cases} (1.290 - 0.024U) \times 10^{-3} (U \le 8 \text{ m/s}) \\ (0.58 + 0.063U) \times 10^{-3} (U > 8 \text{ m/s}) \end{cases} \tag{11}$$

The other is the wave-dependent C_D (Janssen, 1989, 1991). In SuWAT, Mastenbroek, Burgers, and Janssen's iteration (1993) for Janssen's formulation of the exponential wave growth term in wave modules (given in the "Wave Module" section) is used to estimate the wave-dependent C_D. Following his assumption, waves influence the boundary layer: $\tau = \tau_w + \tau_t$, where τ_w is the wave-induced stress, τ_τ is the turbulent stress, and τ is the total stress. The wind profile is given by

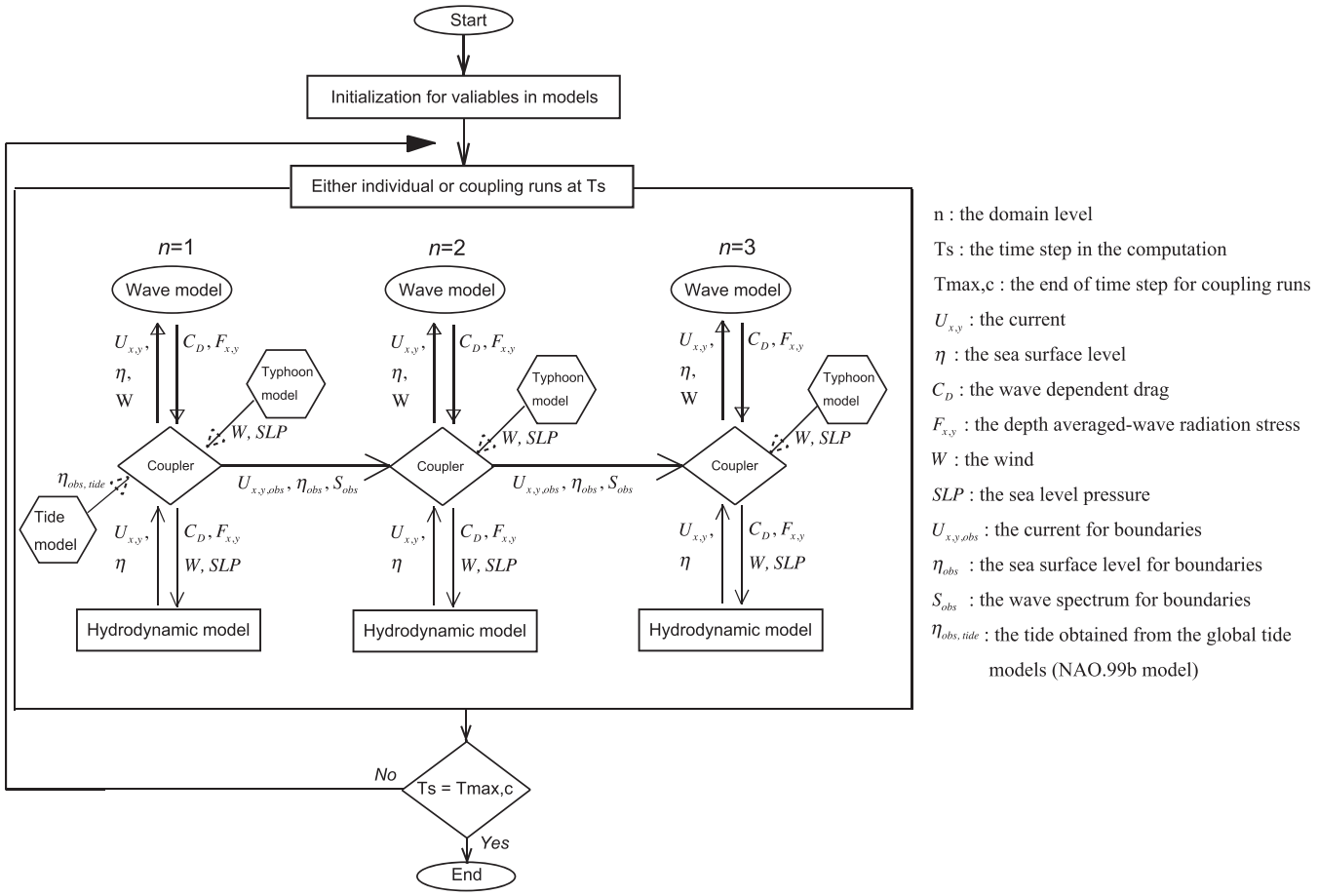

Figure 2. Framework of SuWAT for three level domains that shows the information flow between surge and wave modules in each domain.

$$U(z) = \frac{u_*}{\kappa}\ln\left(\frac{z + z_e + z_0}{z_e}\right) \tag{12}$$

where $U(z)$ is the wind speed at height, z_e is the effective roughness, z_0 is the roughness length, z is the height, and $\kappa = 0.4$ is the von Kármán constant. The turbulent stress is parameterized with a mixing-length hypothesis:

$$\tau_t = \rho_a(\kappa z)^2\left(\frac{\partial U}{\partial z}\right)^2 \tag{13}$$

where ρ_a is the air density.

If the wind profile in Equation (12) is differentiated, squared, and compared with the form in Equation (13), an expression for z_e for $z = z_0$ (Mastenbroek, Burgers, and Janssen, 1993) can be found:

$$z_e = \frac{z_0}{\sqrt{1 - \tau_w - \tau}} \tag{14}$$

where $\tau_w = \tau_w(z_0)$. To parameterize the roughness length z_0, Janssen assumes that a Charnock-like relation $z_0 = \tilde{\alpha}u_*^2/g$ is valid with the values for $u_* = \sqrt{\tau/\rho_a}$ and $\tilde{\alpha} = 0.0081$, which is the Charnock parameter. With the effective roughness (z_e), the wave-dependent C_D is finally obtained by the following equation:

$$C_D = u_*^2/U(z)^2 = \left[\kappa/\ln\left(\frac{z + z_e - z_0}{z_e}\right)\right]^2 \tag{15}$$

In this study, Equation (15) is used to estimate the wind stress in Equation (10) instead of conventional C_D in Equation (11). The effect of leveling off at wind speeds of 22 to 33 m/s on C_D is not taken into account (Donelan *et al.*, 2004; Kim *et al.*, 2015; Powell, Vickery, and Reinhold, 2003).

The solid boundary condition is adopted at land boundaries for no inundation conditions. The radiation condition along open boundaries is given by following Flather's method (1994) in all domains. The current and sea surface level in the coarse grid domain are transferred to the nested open boundaries in the fine grid domain at each time step of 4 s. The time step is 4 s for the surge model.

Tidal Module

The astronomical tide in SuWAT is imposed by a global ocean tide model (Matsumoto, Takanezawa, and Ooe, 2000) that predicts tidal levels for 16 constituents: M2, S2, K1, O1, N2, P1, K2, Q1, M1, J1, OO1, 2N2, Mu2, Nu2, L2, and T2. At every time step, the tidal level is imposed on open boundaries in only the outermost domain. Along the open boundary, the sea surface level is given by

$$\eta = \eta_{tide} + \eta_{surge} \tag{16}$$

where η_{tide} is the tidal level and η_{surge} is the surge level.

Wave Module

The simulating waves nearshore (SWAN) model (Booij, Ris, and Holthuijsen, 1999) integrated in the wave module solves the spectral action balance equation to estimate a wave spectrum (Booij, Ris, and Holthuijsen, 1999). The wave in SuWAT is estimated by time-varying currents and sea surface levels calculated from the surge module. The updated parameters of the wave-dependent drag and the radiation stress in the wave module are returned to the surge module to calculate the current and sea surface level. SWAN version 40.41 has been integrated into SuWAT as the wave module (Kim, Yasuda, and Mase, 2008).

As done in Kim *et al.* (2015), in the present simulation, the default values of parameters for physics are used: Cavaleri and Malanotte-Rizzoli (1981) for linear wave growth, Janssen (1989, 1991) for exponential wave growth, Janssen (1991) for whitecapping, Hasselmann *et al.* (1985) for quadruplet interaction, Battjes and Janssen (1978) for depth-induced breaking, and Madsen, Poon, and Graber (1988) for bottom friction. The diffraction is adapted in the wave calculation. An Ursell number of 10 is used for the limit of the quadruplet interaction, with a factor of 1.0 for the fraction of breaking waves. The following discretizations were used: the direction resolution is 10°, and the frequency range is 0.05 to 1.00 Hz. In the outermost domain, the wave spectrum along open boundaries is estimated by the Joint North Sea Wave Project spectrum, with a peak enhancement parameter of 3.3, the peak period, and a directional width of 10°. The wave spectrum in the coarse grid domain is transferred to the open boundaries in the fine grid domain at each time step of 900 s. The time step is 900 s for the wave model.

Parametric Wind and Pressure Model

A parametric wind and pressure model implemented in the SuWAT model is used to estimate typhoon wind and pressure fields. Schloemer's formula (1954) is used for the pressure:

$$p = p_c + \Delta p\exp(-r_0/r) \tag{17}$$

where p is the atmospheric pressure at distance r from the center, p_c is the central atmospheric pressure, Δp is the difference between p and p_c, and r_0 is the radius to the maximum wind.

Fujii and Mitsuta's formula (1986) for the surface wind is written as follows:

$$V_{gr} = r_t\left(\sqrt{\frac{f^2}{4} + \frac{r_0\Delta p}{\rho_a r^2 r_t}\exp(-r_0/r)} - \frac{f}{2}\right) \tag{18}$$

where V_{gr} is the geostrophic wind and r_t is the following relation:

$$r_t = r\Big/\left(1 + \frac{U_{10}}{V_{gr}}\sin\beta\right) \tag{19}$$

In Equation (19), V_{gr} and U_{10} are at the previous time step. Here, β is the degree between the typhoon moving direction and the direction to r in the anticlockwise direction. U_{10} is calculated by multiplying V_{gr} by $G(x)$ as follows:

$$G(x) = G(\infty) + \left[G(x_p) - G(\infty)\right](x/x_p)^{k-1}\exp(1 - 1/k)\left[1 - (x/x_p)^k\right] \tag{20}$$

$$U_{10} = V_{gr}G(x) \tag{21}$$

where $x = r/r_0$, $k = 2.5$, $x_p = 0.5$, $G(x_p) = 1.2$, and $G(\infty) = 0.667$ are given by Fujii and Mitsuta (1986). In the wind model, the geostrophic wind is reduced by a factor of $G(\infty)$. Finally, the

Table 2. *List of the numerical experiments.*

Typhoons	Simulation Case	Tide	Conventional C_D (without wave effect)	Wave-Dependent Drag	Wave Radiation Stress
Xangsane (2006)	Tide	Yes	No	No	No
	Uncoupled surge with tide	No	Yes	No	No
	Coupled surge with tide	Yes	Yes	No	No
	Uncoupled surge with wave	No	Yes	No	No
	Coupled surge with wave	No	No	Yes	Yes
	Coupled surge without radiation stress	No	No	Yes	No
Ketsana (2009) and Nary (2013)	Uncoupled surge with wave	No	Yes	No	No
	Coupled surge with wave	No	No	Yes	Yes
Historical typhoons (1951–2014)	Coupled surge with wave	No	No	Yes	Yes

wind at a 10-m height is obtained from the vector sum of the wind at a 10-m height calculated by Equation (21) and the typhoon moving speed. In the present model, deformation of the core structure in the typhoon is not considered.

Storm Surge Simulations

A series of numerical experiments is summarized in Table 2. First, to examine interactions of surge and tide and of surge and wave, six cases in Table 2 were carried out for Typhoon Xangsane (2006). For additional examination, the cases of coupled surge with wave and uncoupled surge with wave were conducted for Typhoons Ketsana (2009) and Nary (2013). For the historical storm surge simulations of typhoons from 1951 to 2014, the case of coupled surge with wave was executed.

In the case of tide, only the tide is simulated without typhoon fields of wind and atmospheric pressure. In the cases of uncoupled surge with tide and coupled surge with tide, the storm surge is calculated using the conventional C_D of Honda and Mitsuyasu (1980) in Equation (11). In the case of uncoupled surge with tide, the storm surge is calculated on mean sea level. The case of uncoupled surge with wave is the same as that of uncoupled surge with tide. The case of coupled surge without radiation stress uses the wave-dependent C_D (Janssen, 1989, 1991) in Equation (15) to estimate the wind stress on sea surface layers but excludes the radiation stress. The case of coupled surge with wave includes both the wave-dependent C_D and the radiation stress in the storm surge simulation.

Bathymetry

For numerical simulations, the complexity of the geophysical features was taken into account using the three-level grid system summarized in Table 3, where the outermost domain, D1 (Figure 1a), covers the whole East Sea and the domain D2 (Figure 1b) is set to cover the northern coast of the Province of Quangbinh to the southern coast of the Province of Quangnam. The innermost domain, D3, is focused on the four tidal stations of Cuaviet, Thuanan, Sontra, and Tamky (Figure 1c), where high surge levels (normally larger than 0.5 m) generated. The General Bathymetry Chart of the Ocean of the British Ocean Data Center was used to extract bathymetry for domains D1 and D2. However, coastal topography maps with scales of 1/100,000 published by the Vietnam Administration of Seas and Islands were used for domain D3. As showed in Figure 1, the continental shelf strongly enlarges from south to north. This can be confirmed by Figure 3, where the bed profiles in the cross-shore direction at five stations are shown.

Table 3. *Information on computational domains.*

Domain No.	Computational Domain	Grid Size (m)	No. Grid
D1	105–120° E, 8–22° N	$\Delta x = \Delta y = 7400$	226 × 211
D2	106–111° E, 12–18° N	$\Delta x = \Delta y = 1850$	241 × 301
D3	107.0–109° E, 15.5–17.0° N	$\Delta x = \Delta y = 925$	241 × 181

RESULTS

This section presents results of a series of storm surge hindcasts because of Typhoons Xangsane (2006), Ketsana (2009), and Nary (2013), as summarized in Table 2.

Hindcast of Typhoon Xangsane (2006)

To investigate how the tide influences the storm surge in the study area, a series of simulations were conducted to calculate the Typhoon Xangsane surge. According to the RSMC of JMA, after passing the Philippines, Typhoon Xangsane made landfall on the central coast of Vietnam, causing coastal flooding and landslides. The typhoon was responsible for at least 279 deaths, mostly in the Philippines and Vietnam, and $747 million in damage (Thanh, 2011).

The six hourly synoptic observations of sea-level pressure indicate that the maximum depressions of sea-level pressure are 977 and 993 hPa at Sontra (Figure 4a) and Thuanan (Figure 4b), respectively. Observed winds reached 32 m/s at

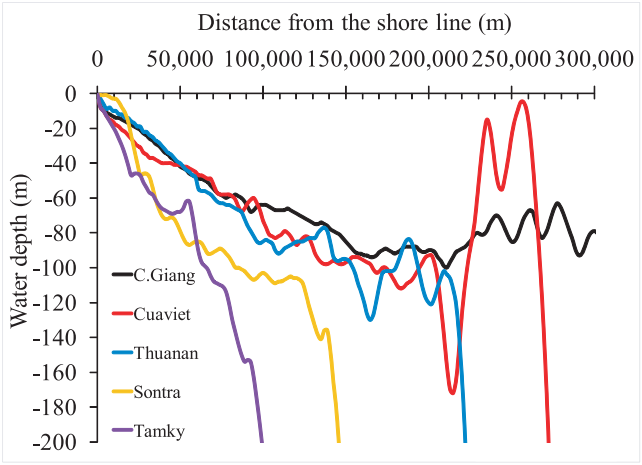

Figure 3. Bed profiles at five locations (Cuagianh, Cuaviet, Thuanan, Sontra, and Tamky). (Color for this figure is available in the online version of this paper.)

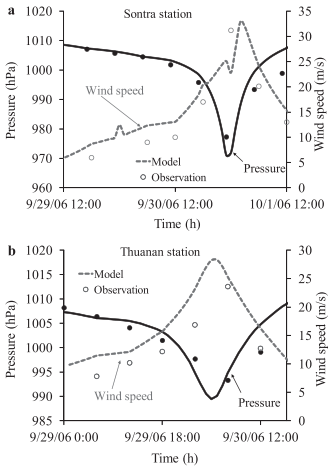

Figure 4. Time series of observed (circle) and calculated (line) winds and atmospheric pressures at the stations of Sontra (a) and Thuanan (b) because of Typhoon Xangsane. The solid line indicates pressure, and the dotted line denotes wind speed. The computations were carried out using the formulae of Schloemer (1954) and Fujii and Mitsuta (1986) for atmospheric pressure and wind, respectively.

Sontra (Figure 4a). Calculated wind and pressure fields were slightly overestimated within the absolute errors of 10%; however, it is believed that overall the estimated wind and pressure fields are acceptable to calculate the Typhoon Xangsane surge.

In the numerical experiment, a series of three simulations of tide, uncoupled surge with tide, and coupled surge with tide

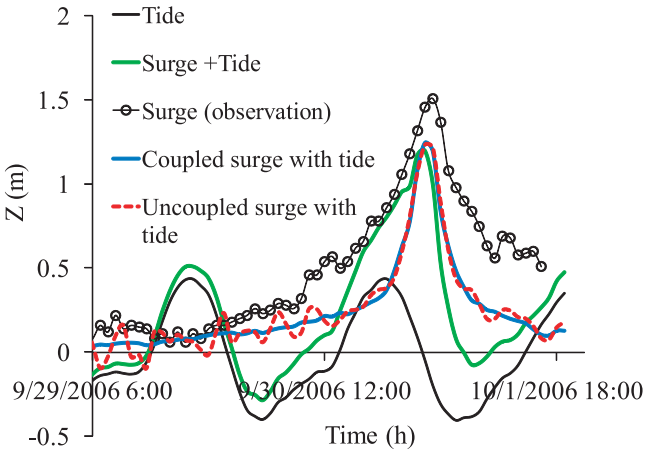

Figure 5. Time series of calculated tides only (tide), calculated surges coupled with tides (surge + tide), observed surges (observation), surges extracted from surge+tide (coupled surge with tide), and calculated surge on mean sea level (uncoupled surge with tide) at Sontra during Typhoon Xangsane. The storm surge simulations either including the tide (coupled surge with tide in Table 2) or excluding one (uncoupled surge with tide in Table 2) were conducted using the conventional drag of Honda and Mitsuyasu (1980). The use of conventional drag underestimated the surge heights regardless of the tide. (Color for this figure is available in the online version of this paper.)

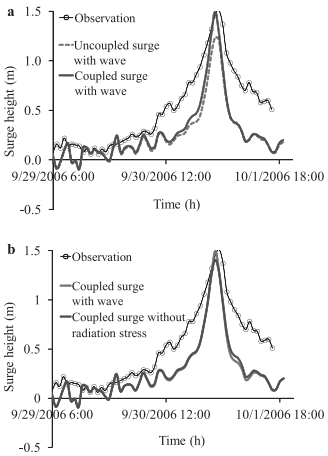

Figure 6. Time series of storm surge heights at Sontra. (a) In a series of simulations, the wave-dependent drag and radiation stress are included in the case of coupled surge with wave, while only the conventional drag is used in the case of uncoupled surge with wave. The calculation results indicate the inclusion of the wave-dependent drag and radiation stress improves surge heights. (b) The case of coupled surge with wave is the same as the case in (a). However, the radiation stress is ignored in the case of coupled surge without radiation stress. The radiation stress affected the surge height at peak.

were conducted. The cases of uncoupled surge with tide and coupled surge with tide listed in Table 2 used conventional C_D (Honda and Mitsuyasu, 1980) to estimate the wind stress without the wave impact of the radiation stress and wave-dependent drag. First, the case of coupled surge with tide in Table 2 was carried out to calculate the Typhoon Xangsane surge. Second, the tidal simulation in the case of tide was conducted to extract the surge level ($\eta_{surge,1}$, the case of coupled surge with tide in Figure 5), taking into account the surge and tide interaction as follows: $\eta_{surge,1} = \eta_{tide} + \eta_{surge}$. Finally, the case of uncoupled surge with tide was executed on mean sea level.

The results of the series of simulations are shown in Figure 5, which presents comparisons between observations and calculations at Sontra. From the simulation results, there are discrepancies between the surge levels with and those without the tide from 29 to 30 September. However, two surge levels seem to be identical from 30 September. In addition, the use of conventional C_D is not enough to simulate the observations, regardless of the consideration of the surge and tide interaction. As a result, it was found that the tidal effect is insignificant in the surge level on the coast of the study area.

Next, additional calculations on mean sea level were carried out by coupling the wave. As listed in Table 2, the case of coupled surge with wave considered the wave-dependent drag and radiation stress, while the case of coupled surge without radiation stress excluded the radiation stress. Then, results were compared with those obtained from the case of uncoupled surge with wave that uses conventional C_D on mean sea level, as shown in Figure 6. As shown in Figure 6a, the peak surge level calculated with the wave-dependent drag and radiation stress is improved and in close agreement with the observation at Sontra. The difference between the two cases at the peak

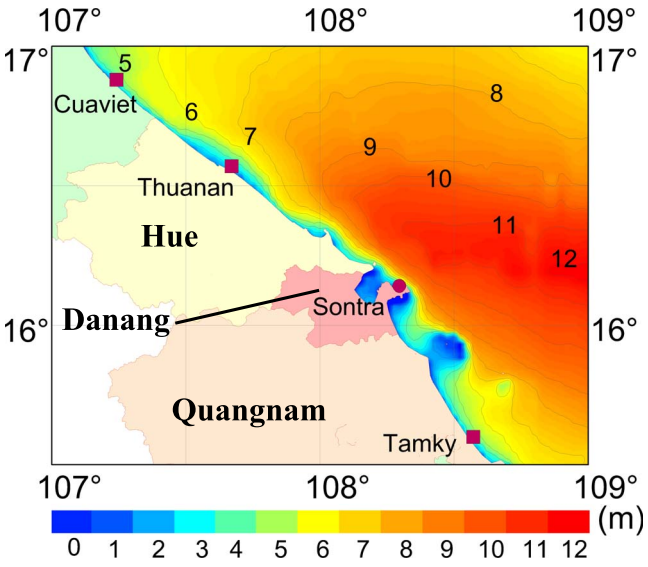

Figure 7. Maximum significant wave heights in the innermost domain because of Typhoon Xangsane. The simulation considered the wave-dependent drag and radiation stress. (Color for this figure is available in the online version of this paper.)

levels is 0.3 m. This suggests that the surge and wave interaction improves the surge level.

To clarify whether the wave-dependent drag or the radiation stress is more critical, the result of coupled surge with wave was compared to that of coupled surge without radiation stress as shown in Figure 6b. Comparing two surges, it was found that the surge level is underestimated, especially, at peak, when the radiation stress is ignored. The difference between both peak levels is 0.1 m. The results depicted that the calculated surge levels are overall underestimated except around the peak surge levels. These results may be due to underestimation of the wave setup estimated on the coarse resolutions, because the wave breaking was not fully solved in the innermost domain with the 1-km grid size, as shown in Figure 7. The maximum significant wave heights of larger than 12 m come from offshore and break nearshore, depending on the bed slopes, as seen in

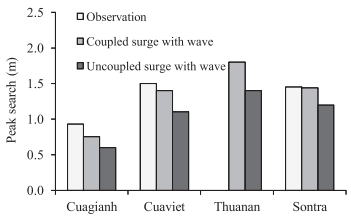

Figure 8. Comparisons of the observed peak surge levels (observation), the calculated ones including the wave-dependent drag and radiation stress (coupled surge with wave), and the calculated ones excluding both (uncoupled surge with wave) at Cuagianh, Cuaviet, Thuanan, and Sontra because of Typhoon Xangsane. The peak surge levels calculated with the wave-dependent drag and radiation stress were in good agreement with the observed ones. There is no observation at Thuanan.

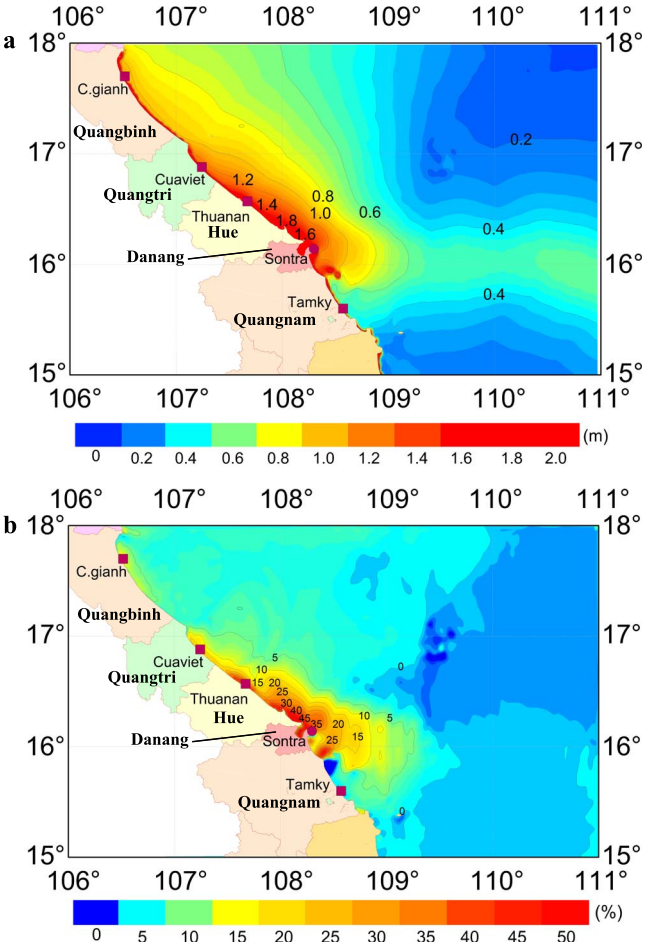

Figure 9. (a) Spatial distributions of the peak surge levels because of Typhoon Xangsane when considering the factors of wave-dependent drag, radiation stress, and atmospheric pressure. (b) The maximum contributions of the wave-dependent drag and radiation stress to the total surge levels as percentages. The impact of the wave-dependent drag and radiation stress reached up to 45% in total surge level along the coast. (Color for this figure is available in the online version of this paper.)

Figure 3. In addition, it might arise from the horizontal two-dimensional simplification to represent the Ekman transport in moderate water depth (*e.g.*, Bertin *et al.*, 2015). This problem would be solved when using a three-dimensional model.

Figure 8 shows comparisons of the observed and calculated peak surge levels in the cases of coupled surge with wave and uncoupled surge with wave at four stations. The results show that in the case of coupled surge with wave, considering the wave effect makes an improvement in the accuracy of storm surge simulation at all stations in comparison with the case of uncoupled surge with wave (except at Thuanan because of no observations). Figure 9a shows the spatial distribution of the peak surge levels in the case of coupled surge with wave that combined the wave-dependent drag and the radiation stress. It could be found that the maximum surge level reaches up to 1.8 m on the coast. In addition, the maximum contribution of the

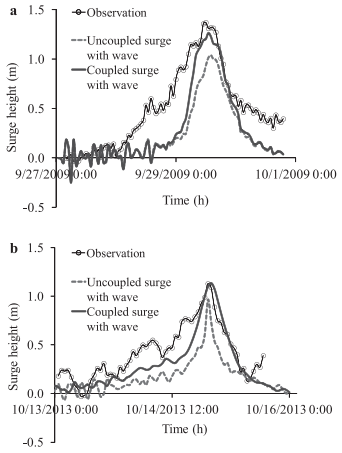

Figure 10. Time series of observed and calculated surge heights at Sontra station because of Typhoon Ketsana (a) and Typhoon Nary (b). In a series of simulations, the wave-dependent drag and radiation stress were included in the case of coupled surge with wave, while only the conventional drag is used in the case of uncoupled surge with wave. The calculated surge heights show that the wave impact was significant in the surge simulation.

wave-generated surge to the total surge level is larger than 45% nearshore (Figure 9b).

Hindcasts of Typhoons Ketsana (2009) and Nary (2013)

Additional simulations of the Typhoon Ketsana and Typhoon Nary surges were conducted that generated storm surges in the study area. In these simulations, two conditions in Table 2 were taken into account on mean sea level: (1) the uncoupled model of uncoupled surge with wave (the use of the conventional drag without the surge–wave interaction) and (2) the coupled model of coupled surge with wave (the use of the wave-dependent drag and the radiation stress). From the results of these simulations, a similar tendency was found that the uncoupled model underestimates the Ketsana (Figure 10a) and Nary (Figure 10b) surges at Sontra, while the coupled model estimates of the surge are in good agreement with observations. Similar to the Typhoon Xangsane surge, the influence of the surge–wave interaction is significant on the storm surge in both typhoons.

Historical Storm Surge on the Coast

Because of lack of observations for the storm surge in this region, information on historical storm surge levels has been needed for planning coastal facilities and mitigating potential coastal damage induced by the impact of climate change. To assess the historical storm surge in the area, a series of storm surge simulations were carried out for the historical typhoons in the period of 1951 to 2014, which uses all available typhoon data from the RSMC of JMA. The trajectories of the typhoons that struck the middle coast of Vietnam over these 63 years are shown in Figure 11. Among them, 49 typhoons were chosen for the storm surge simulations. In the simulations, tide was ignored because the tide–surge interaction is insignificant, as described in the previous section; only the surge–wave interaction, combined with the wave-dependent drag and the radiation stress in the case of coupled surge with wave, was considered.

According to JMA, Typhoon Harriet (1971) was the most intensive typhoon; this hit the Quangtri Province along the track shown in Figure 1b. In Figure 12a, a time series of the Typhoon Harriet wind speed and sea-level pressure at Cuaviet in the Province of Quangtri is shown. It can be seen that the wind and pressure parametric model estimates the Typhoon Harriet wind and pressure field, reaching 45 m/s and 950 hPa, respectively, at Cuaviet. In Figure 12b, a time series of the Typhoon Harriet surge levels is seen, obtained from the coupled model of surge and wave considering the wave-dependent drag and radiation stress. The results show that the peak surge level is larger than 4.0 m. Even though the calculations cannot be validated because of lack of observations, these results of the historical storm surge are reliable based on those of the coupled model validated in the previous sections. The coupled model of surge and wave estimated surges from other typhoons (*e.g.*, Typhoons Cecil, 1975, and Betty, 1987) that are larger than 2.0 m on the coast where the typhoons hit, although the results are not shown here.

DISCUSSION

This section provides discussion of the impact of the tide and the wave and then an assessment of historical storm surges because of the typhoons in the period of 1951 to 2014.

Impact of Tide–Surge Interaction

In the surge simulations of Typhoon Xangsane (2006), it was found that the difference in the surge levels between uncoupled surge with tide and coupled surge with tide was small, probably coming from low tidal ranges below 1.0 m, as seen in Figure 5, for instance. As a result, it can be said that the tidal effect is insignificant in the surge level on the Danang coast of Vietnam. However, on the northern and southern coasts in the Provinces of Quangbinh and Quangnam, the tidal ranges reach up to 2.0 m. For further discussion on the tide–surge interaction, scenario-based typhoons were taken into account: a modeled typhoon that has the same intensity and track as Typhoon Xangsane but makes landfall in both provinces at different tidal phases of 0.9, 0.5, 0, –0.5, and –0.9 m, resulting in the generation of maximum surge levels at the designated tidal phase. In these simulations, two models were used: (1) the uncoupled model of uncoupled surge with wave and (2) the coupled model of coupled surge with wave, as listed in Table 2. The tide–surge interaction was examined at Cuagianh and Tamky in both provinces, as shown in Figure 13. From the results of the uncoupled and coupled models, the peak surge level decreases slightly as the tide phase and current increase. However, the change of the peak surge level against the tide phase is within 2%, as found at Sontra in the "Hindcast of Typhoons Xangsane (2006)" section. These results are in line with results reported by Kim, Yasuda, and Mase (2008). In other words, it can be said that the tide–surge interaction is insignificant on the middle coast of Vietnam because of the small tide amplitude.

Impact of Surge–Wave Interaction

In the "Hindcast of Typhoons Xangsane (2006)" section, it was found from the series of numerical experiments that the

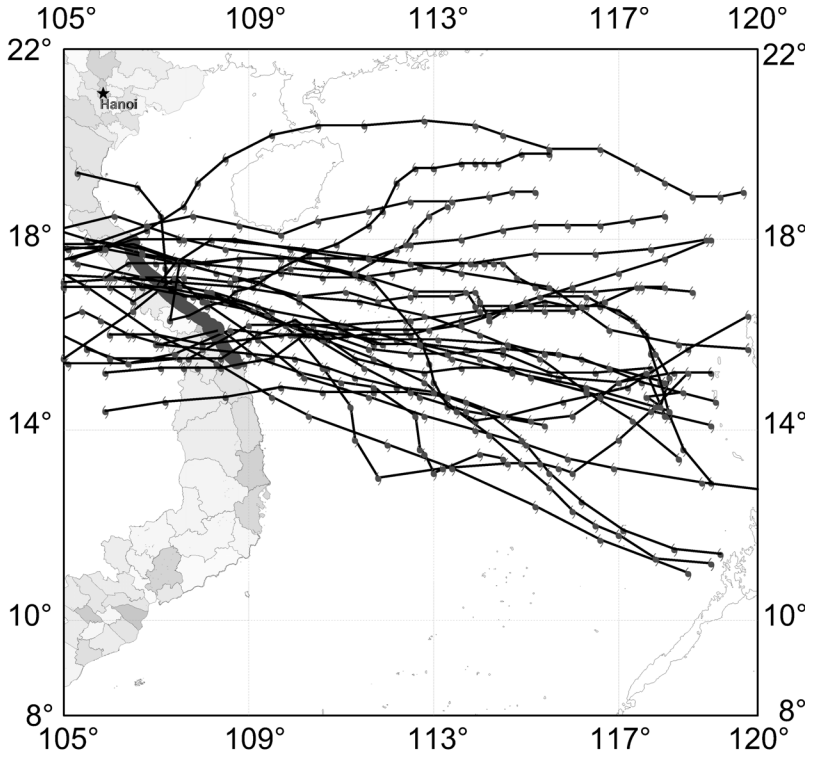

Figure 11. The trajectory of typhoons in the period of 1951 to 2014 that hits the study region.

surge–wave interaction is critical to the estimation of the Typhoon Xangsane surge on the middle coast of Vietnam. In other words, the effect of the wave, combined with the wave-dependent drag and the radiation stress, is the predominant factor affecting the surge level, and its maximum contribution is 45% of the total surge level. At Sontra, the wave-dependent drag contributes approximately 14% to the total surge level, in comparison with the bulk formula. The radiation stress is in

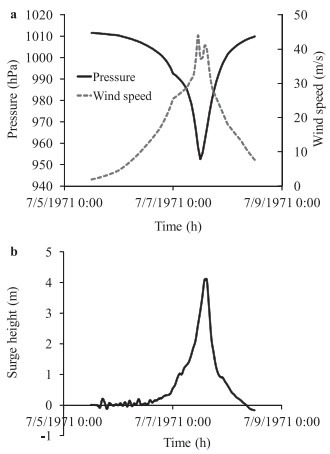

Figure 12. (a) Time series of atmospheric pressures and wind speeds at Cuaviet because of Typhoon Harriet, estimated by formulae of Schloemer (1954) and Fujii and Mitsuta (1986). (b) Time series of storm surges calculated by the surge–wave interaction at Cuaviet because of Typhoon Harriet. The typhoon winds and pressures reached 45 m/s and 950 hPa, respectively, at Cuaviet. The surge height was estimated to be approximately 4.1 m.

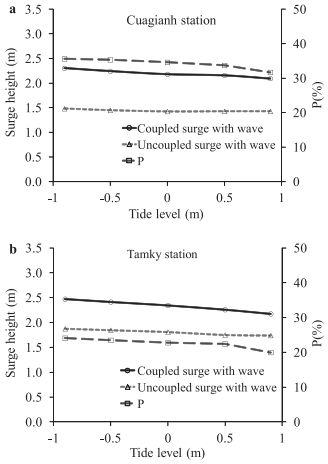

Figure 13. Changes of peak surge levels against different tidal phases at Cuagianh (a) and Tamky (b) in the cases of coupled surge with wave that combined the wave-dependent drag and radiation stress and uncoupled surge with wave that excluded both. In addition, the improvement of the peak surge level in the coupled surge with wave against that in the uncoupled surge with wave is shown as a percentage (P). The results show that the tide–surge interaction is insignificant in terms of tidal phase.

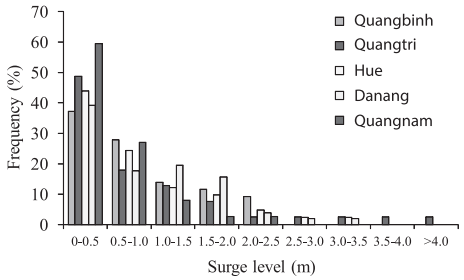

Figure 14. Frequencies of surge levels at five provinces in the period of 1951 to 2014. The figure shows the reproduction of the frequency of peak surge heights using the surge and wave coupled model.

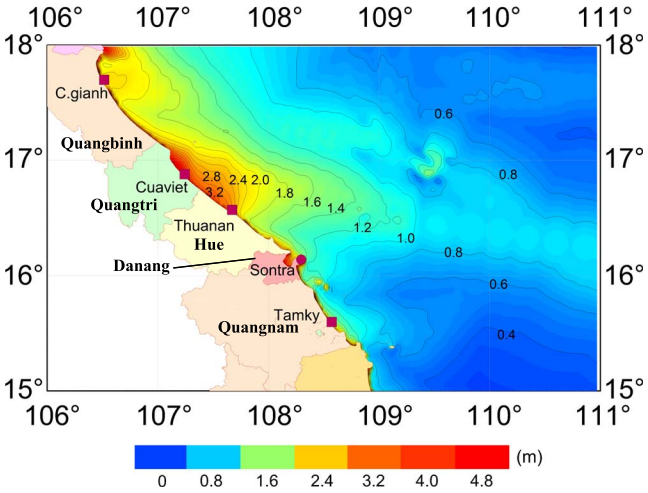

Figure 15. Distributions of maximum surge levels on the coast from Quangbinh to Quangnam in the period of 1951 to 2014. The figure shows that the highest peak surge levels of larger than 3.0 m were concentrated on the Provinces of Quangtri, Hue, and Danang because of the most intensive typhoon, Harriet. (Color for this figure is available in the online version of this paper.)

charge of up to approximately 7% of the difference in the total surge level between the simulations including the wave-dependent drag and radiation stress and only the wave-dependent drag. Similar to Typhoon Xangsane, from the storm surge simulations of Typhoon Ketsana, the wave impact contributes up to 25% to the total surge level. In Typhoons Ketsana and Nary, the wave-dependent drag is in charge of maximally 16% in the total surge level compared to using only the bulk formula, while the radiation stress is responsible for up to 9% of the difference between the total surge levels obtained from using both the wave-dependent drag and the radiation stress and those obtained from using only the wave-dependent drag (the results are not shown here). Therefore, the importance of the surge–wave interaction in the present study is affirmed from the surge simulations of three typhoon surges of Typhoons Xangsane, Ketsana, and Nary. In addition, the surge–wave interaction significantly influences the peak surge level in all simulations, as found in the previous sections. Furthermore, the results indicate that the effect of the wave varies with locations: the highest percentage of the wave-generated surge in total surge at Cuagianh is 35% at the lowest tidal phase (Figure 13a), while that at Tamky is 24% (Figure 13b).

Analysis of Historical Storm Surge on the Coast

Based on the results of the historical storm surge simulations presented in the "Results" section, a frequency analysis of the surge levels for five provinces was carried out as shown in Figure 14. As a result, surge levels of smaller than 0.5 m predominantly appear in each province. In the Provinces of Quangtri, Hue, and Danang, surge levels of larger than 2.5 m appear. Especially, in Quangtri, the highest surge level of 4.1 m because of Typhoon Harriet (1971) was estimated. However, surge levels of less than 2.5 m occurred in the Provinces of Quangbinh and Quangnam. The spatial distribution of the highest peak surge level during the period of 1951 to 2014 is provided in Figure 15. It is seen that overall, the highest peak surge levels of more than 2.0 m mainly occurred along the coast. In particular, the highest peak surge levels of larger than 3.0 m are concentrated on the coasts of the Quangtri, Hue, and Danang Provinces because of the landfall of Typhoon Harriet, which was the most intense typhoon in these regions. It is believed that these results are useful in practice for designing coastal facilities such as dikes and breakwaters and provide elementary information on planning mitigation of climate change impacts on the coastal zone in Vietnam.

CONCLUSIONS

In recent years, the activity of TCs has accelerated; as a result, the weather and hydrological phenomena in Vietnam have become more variable (*e.g.*, Tan and Thanh, 2013). To mitigate future storm surge damage, it is important to understand features of storm surges on the coast of central Vietnam. In the present study, assessment of extreme surge levels because of historical typhoons in the period of 1951 to 2014 is conducted. Before the assessment, the interaction of surge, wave, and tide is investigated to look for a predominant factor that contributes to storm surge generation on the middle coast of Vietnam during typhoon events. A series of storm surge simulations is conducted using SuWAT (Kim, Yasuda, and Mase, 2008). A parametric wind and pressure model is employed to estimate typhoon wind and pressure fields.

First, the interaction of surge and tide is investigated during Typhoon Xangsane (2006). Results that the tide–surge interaction is negligible, with a difference of 2% between the surge levels with and those without the tide. Then, the surge–wave interaction is examined for the same typhoon. For the surge–wave interaction, the two factors of wave-dependent drag and wave-induced radiation stress are focused on in the surge simulation. The results show that the wave-dependent drag influences the surge level: maximally 14% in the total surge level. The radiation stress also contributes to the surge level: up to 7% in the total surge level. From the series of storm surge simulations for Typhoons Ketsana (2009) and Nary (2013), it is also shown that the surge–wave interaction combining the wave-dependent drag and the radiation stress contributes up to

25% to the total surge level and is crucial to the simulation of the storm surge. As a result, it is found that the predominant factor is the wave-dependent drag in the storm surge simulation that takes into account the surge–wave interaction. In addition, it reveals that the radiation stress is a substantial factor.

Using the coupled model of surge and wave, a series of the historical storm surge simulations in the period of 1951 to 2014 is conducted to assess the storm surge on the middle coast of Vietnam because of lack of observations. From this period, 49 typhoons are selected. The results indicate that in the study area, surge levels of 2.0 to 2.5 m are predominant on the coasts of the Provinces of Quangbinh to Danang. Surge levels larger than 3.0 m are concentrated on the coasts of the Provinces of Quangtri, Hue, and Danang: in particular, the highest surge level of 4.1 m occurs in Quangtri because of Typhoon Harriet (1971). It is believed that these results provide elementary information on planning and designing coastal facilities and mitigations for potential supertyphoons due to climate change impacts on the coastal zone in Vietnam.

In the present study, the relatively coarse grid size of 925 m on the innermost domain was used to look at the effect of the radiation stress on the storm surge. However, the spatial resolution should be increased to more accurately examine the effect of the radiation stress (*e.g.*, Kennedy *et al.*, 2012). Hence, further studies should be done on higher resolutions of less than 1-km grid sizes when planning and managing coastal facilities and structures. In addition, the present study does not consider a wind speed–capped drag at 25 to 30 m/s in the surge and wave interaction in the sea surface boundary (*e.g.*, Kim *et al.*, 2015). A surge–wave interaction in the bottom boundary is not taken into account. Therefore, further studies considering these would be needed to assess supertyphoon-induced surges.

ACKNOWLEDGMENTS

This research is funded by Vietnam National Foundation for Science and Technology Development (NAFOSTED) under grant 105.12-2012.02, partially supported by Japan Society for the Promotion of Science KAKENHI in Japan and the Norwegian Ministry for Foreign Affairs (L.R.H. and C.W.).

LITERATURE CITED

Battjes, J.A. and Janssen, J.P.F.M., 1978. Energy loss and set-up due to breaking of random waves. *Proceeding of 16th International Conference Coastal Engineering* (ASCE), pp. 569–587.

Bertin, X.; Li, K.; Roland, A., and Bidlot, J.R., 2015. The contribution of short waves in storm surges: two recent examples in the central part of the Bay of Biscay. *Continental Shelf Research*, 96, 1–15.

Booij, N.; Ris, R.C., and Holthuijsen, L.H., 1999. A third-generation wave model for coastal regions. Part I: Model description and validation. *Journal of Geophysical Research,* 104(C4), 7649–7666.

Cavaleri, L. and Malanotte-Rizzoli, P., 1981. Wind wave prediction in shallow water: Theory and applications. *Journal of Geophysical Research,* 86(c11), 10961–10973.

Chen, Q.; Wang, L., and Zhao, H., 2008. An integrated surge and wave modeling system for Northern Gulf of Mexico: Simulations for Hurricanes Katrina and Ivan. *Proceedings of the 31st International Conference on Coastal Engineering* (Hamburg, Germany), Vol. 2, pp. 1072–1084.

Chien, D.D., 2015. Researching the Scientific Basis to Assess the Storm Surge in the Sea Areas from Quang Binh to Quang Nam. Hanoi, Vietnam: University of Science–Vietnam National University, Ph.D. dissertation, 117p [in Vietnamese].

Choi, B.H.; Eum, H.M., and Woo, S.B., 2003. A synchronously coupled tide–wave–surge model of Yellow Sea. *Coastal Engineering,* 47, 381–398.

Dietrich, J.C.; Bunya, S.; Westerink, J.J.; Ebersole, B.A.; Smith, J.M.; Atkinson, J.H.; Jensen, R.; Resio, D.T.; Luettich, R.A.; Dawson, C.; Cardone, V.J.; Cox, A.T.; Powell, M.D.; Westerink, H.J., and Roberts, H.J., 2010. A high resolution coupled riverine flow, tide, wind, wind wave and storm surge model for southern Louisiana and Mississippi: Part II—Synoptic description and analyses of Hurricanes Katrina and Rita. *Monthly Weather Review,* 138, 378–404.

Donelan, M.A.; Haus, B.K.; Reul, N.; Plant, W.J.; Stianssnie, M.; Graber, H.C.; Brown, O.B., and Saltzman, E.S., 2004. On the limiting aerodynamic roughness of the ocean in very strong winds. *Geophysical Research Letters,* 31, L18306. doi:10.1029/2004GL019460

Field, C.B.; Barros, V.R.; Dokken, D.J.; Mach, K.J.; Mastrandrea, M.D.; Bilir, T.E.; Chatterjee, M.; Ebi, K.L.; Estrada, Y.O.; Genova, R.C.; Girma, B.; Kissel, E.S.; Levy, A.N.; MacCracken, S.; Mastrandrea, P.R., and White, L.L., 2014. *Climate Change 2014: Impacts, Adaptation, and Vulnerability. Part A: Global and Sectoral Aspects. The Fifth Assessment Report of the Intergovernmental Panel on Climate Change*. Cambridge, U.K.: Cambridge University Press, 1132p.

Flather, R.A., 1994. A storm surge prediction model for the northern Bay of Bengal with application to the cyclone disaster in April 1991. *Journal of Physical Oceanography,* 24, 172–190.

Fujii, T. and Mitsuta, Y., 1986. Synthesis of a stochastic typhoon model and simulation of typhoon winds. *Annuals of the Disaster Prevention Research Institute,* 29(B-1), 229–239 [in Japanese].

Funakoshi, Y.; Hagen, S.C., and Bacopoulos, P., 2008. Coupling of hydrodynamic and wave models: Case study for Hurricane Floyd (1999) hindcast. *Journal of Waterway, Port, Coastal, and Ocean Engineering,* 134(6), 321–335. doi:10.1061/(ASCE)0733-950X

Hasselmann, S.; Hasselmann, K.; Allender, J.H., and Barnett, T.P., 1985. Computations and parameterizations of the nonlinear energy transfer in a gravity wave spectrum. Part II: Parameterizations of the nonlinear transfer for application in wave models. *Journal of Physical Oceanography,* 15(11), 1378–1391.

Hien, N.X.; Uu, D.V.; Thuc, T., and Tien, P.V., 2010. Study on wave setup with the storm surge in Hai Phong coastal and estuarine region. *Vietnam National University Journal of Science, Earth Sciences,* 26, 82–89.

Honda, T. and Mitsuyasu, H., 1980. Experimental study of wind stress in the sea surface. *Annual Journal of Coastal Engineering,* 27, 90–93 [in Japanese].

Janssen, P.A.E.M., 1989. Wave-induced stress and the drag of air flow over sea waves. *Journal of Physical Oceanography,* 19, 745–754.

Janssen, P.A.E.M., 1991. Quasi-linear theory of wind-wave generation applied to wave forecasting. *Journal of Physical Oceanography,* 21, 1631–1642.

JMA (Japan Meteorological Agency), 2016. *RSMC Best Track Data*. http://www.jma.go.jp/jma/jma-eng/jma-center/rsmc-hp-pub-eg/besttrack.html.

Kennedy, A.B.; Westerink, J.J.; Smith, J.M.; Hope, M.E.; Hartman, M.; Taflanidis, A.A.; Tanaka, S.; Westerink, H.; Cheung, K.F.; Smith, T.; Hamann, M.; Minamide, M.; Ota, A., and Dawson, C., 2012. Tropical cyclone inundation potential on the Hawaiian Islands of Oahu and Kauai. *Ocean Modelling,* 52–53, 54–68. doi:10.1016/j.ocemod.2012.04.009

Kim, S.Y.; Matsumi, Y.; Yasuda, T., and Mase, H., 2014. Storm surges along the Tottori coasts following a typhoon. *Ocean Engineering,* 91, 133–145.

Kim, S.Y.; Mori, N.; Mase, H., and Yasuda, T., 2015. The role of sea surface drag in a coupled surge and wave model for Typhoon Haiyan 2013. *Ocean Modelling,* 96(1), 65–84. doi:10.1016/j.ocemod.2015.06.004

Kim, S.Y.; Yasuda, T., and Mase, H., 2008. Numerical analysis of effects of tidal variations on storm surges and waves. *Applied Ocean Research,* 30, 311–322.

Kim, S.Y.; Yasuda, T., and Mase, H., 2010. Wave set-up in the storm surge along open coasts during Typhoon Anita. *Coastal Engineering,* 57, 631–642.

Madsen, O.S.; Poon, Y.K., and Graber, H.C., 1988. Spectral wave attenuation by bottom friction: Theory. *Proceeding of 21st International Conference Coastal Engineering* (ASCE), pp. 492–504.

Mase, H.; Muto, R.; Mori, N.; Kim, S.Y.; Yasuda, T., and Hayashi, Y., 2011. Storm surge simulation due to Isewan Typhoon using detail meteorological re-analysis data. *Journal of Japan Society of Civil Engineers, Series B2* (*Coastal Engineering*), 67(2), 401–405 [in Japanese].

Mastenbroek, C.; Burgers, G., and Janssen, P.A.E.M., 1983. The dynamical coupling of a wave model and a storm surge model through the atmospheric boundary layer. *Journal of Physical Oceanography,* 23, 1856–1866.

Matsumoto, K.; Takanezawa, T., and Ooe, M., 2000. Ocean tide models developed by assimilating TOPEX/POSEIDON altimeter data into hydrodynamical model: A global model and a regional model around Japan. *Journal of Oceanography,* 56, 567–581.

Ninh, P.V., 1992. The Storm Surge Models. *UNDP Project VIE/87/020*, Hanoi, Vietnam: Institute of Mechanics, 147p.

Powell, M.D.; Vickery, P.J., and Reinhold, T.A., 2003. Reduced drag coefficient for high wind speeds in tropical cyclones. *Nature,* 422, 279–283.

Sao, N.T., 2008. Storm surge predictions for Vietnam coast by Delft3D model using results from RAMS model. *Journal of Water Resources and Environmental Engineering,* 23, 39–47.

Schloemer, R.W., 1954. *Analysis and Synthesis of Hurricane Wind Patterns over Lake Okechobee*. Washington, D.C.: U.S. Government Printing Office, *Report No. 31,* 49p.

Tan, P.V. and Thanh, N.D., 2013. Climate change in Vietnam: Some research findings, challenges and opportunities in international integration. *Vietnam National University Journal of Science,* 29, 42–55 [in Vietnamese, abstract in English].

Thang, N.V., 1999. Building Scheme for Storm Surge Prediction in Hai Phong Coastal Zone. Hanoi, Vietnam: Vietnam Institute of Meteorology, Hydrology and Environment, Ph.D. dissertation, 120p [in Vietnamese].

Thanh, H.T., 2011. The Variation of Sea Level in Coastal Zone of Vietnam. Hanoi, Vietnam: Institute of Meteorology, Hydrology and Environment, Ph.D. dissertation, 91p [in Vietnamese].

Thuy, N.B.; Cuong, H.D.; Tien, D.D.; Chien, D.D., and Kim, S.Y., 2014. Assessment of changes in sea-level caused by Typhoon No. 3 in 2014 and forecast problems. *Scientific and Technical Hydro-Meteorological Journal,* 647, 16–20 [in Vietnamese].

Thuy, V.T.Th., 2003. Storm Surge Modeling for Vietnam's Coast. Delft, The Netherlands: Delft Hydraulic, Master's thesis, 140p.

WMO (World Meteorological Organization) Staff, 1998. *Guide to Wave Analysis and Forecasting,* 2nd edition, *WMO-No. 702*. Geneva, Switzerland: Secretariat of the World Meteorological Organization, 159p.

Zhang, M.Y. and Li, Y.S., 1997. The dynamic coupling of a 3rd-generation wave model and a 3D hydrodynamic model through boundary-layers. *Continental Shelf Research,* 17, 1141–1170.